Materials Letters 228 (2018) 96–99

Contents lists available at ScienceDirect

Materials Letters

journal homepage: www.elsevier.com/locate/mlblue

Featured Letter

$LiYGeO_4$: Novel low-permittivity microwave dielectric ceramics with intrinsic low sintering temperature

Kai Cheng [a,c], Chunchun Li [a,b,*], Huaicheng Xiang [a], Yihua Sun [c], Liang Fang [a,*]

[a] Guangxi Universities Key Laboratory of Non-ferrous Metal Oxide Electronic Functional Materials and Devices, College of Material Science and Engineering, Guilin University of Technology, Guilin 541004, China

[b] College of Information Science and Engineering, Guilin University of Technology, Guilin 541004, China

[c] College of Materials and Chemical Engineering, Three Gorges University, Yichang 443002, China

ARTICLE INFO

Article history:
Received 26 April 2018
Received in revised form 27 May 2018
Accepted 28 May 2018
Available online 1 June 2018

Keywords:
Ceramics
Dielectrics
Low permittivity
Olivine structure
Low-temperature co-fired ceramics

ABSTRACT

Using the solid-state reaction route, a new low-firing microwave dielectric ceramic $LiYGeO_4$ was prepared, and the phase evolution, thermal stability, and dielectric properties were characterized. A single orthorhombic phase $LiYGeO_4$ formed in the sintering temperature range of 920–960 °C decomposed into Y_2GeO_5, GeO_2, and Li_2O when the sintering temperature exceeded 960 °C. $LiYGeO_4$ densified at 940 °C/6 h possessed a relative permittivity 9.41, a quality factor 18,860 GHz (at 12.8 GHz), and a temperature coefficient of resonant frequency −27.7 ppm/°C. The negative τ_f value was compensated by compositing with $CaTiO_3$, and $0.97LiYGeO_4$-$0.03CaTiO_3$ ceramic exhibited a near-zero τ_f of −1.37 ppm/°C along with a permittivity of 9.83 and a quality factor of 12,940 GHz (at 13.2 GHz). All merits make $LiYGeO_4$ a promising candidate for high-frequency communication application, and low-temperature co-fired ceramics.

1. Introduction

Recently, the explosive growth of communication technologies has expanded the operating frequency to millimeter wave range to fulfill the quantity and speed of data transmission [1,2]. Transmission speed is importantly related to the signal propagation that is positively correlated with the relative permittivity [3]. Hence, low-ε_r ($\varepsilon_r < 15$) dielectric ceramics available are strongly demanded to avoid signal propagation delay and also to minimize the cross-coupling with conductors. Moreover, low-temperature co-fired ceramics (LTCC) technology offers benefits in the fabrications of miniature multilayered devices, which also need low-ε_r materials as subtracts [4]. Hence, low-ε_r materials with high performances are strongly demanded in high-frequency and LTCC applications.

Over the past decades, some olivine structured materials A_2BO_4, e.g., Li_2AGeO_4 (A = Zn, Mg), M_2GeO_4 and M_2SiO_4 (M = Zn, Mg), have been reported as promising candidates for low-ε_r dielectric materials [5–9]. It is safe to speculate that their low permittivities derive from low ionic polarizability of the constitution ions, such as Si (0.87 Å^3) and Ge (1.63 Å^3). Besides, most of the low-ε_r materials have high sintering temperature or large $|\tau_f|$ values, which would to some extent restrict their practical applications. Furthermore, Li-containing oxides have been reported as low-firing ceramics, e.g., Li_4WO_5, $Li_4Mg_3Ti_2O_9$, and $Li_2ZnGe_3O_8$ [10–12]. Therefore, a Li-containing olivine compound $LiYGeO_4$ was prepared and characterized to seek low-ε_r dielectric materials with intrinsic low sintering temperature. The phase evolution, thermal stability, sintering behavior, and microwave dielectric properties were investigated in detail.

2. Experimental

$LiYGeO_4$ ceramics were prepared by the solid-state method and the processing procedure is similar as described in our previous work (details in supplementary information) [6]. Before weighting, Y_2O_3 powders were dried at 1000 °C for 2 h. The calcining temperature was 880 °C, and the sintering temperature ranged from 920 °C to 1000 °C for 6 h with a heating rate of 5 °C/min. Composite ceramics between $LiYGeO_4$ and $CaTiO_3$ were prepared with general formula $(1-x)LiYGeO_4$-$xCaTiO_3$ ($0 \le x \le 0.045$) to adjust the thermal stability, which sintered in the temperature range of 900–960 °C for 6 h.

* Corresponding authors at: Guangxi Universities Key Laboratory of Non-ferrous Metal Oxide Electronic Functional Materials and Devices, College of Material Science and Engineering, Guilin University of Technology, Guilin 541004, China (C. Li).

E-mail addresses: lichunchun2003@126.com (C. Li), fanglianggl001@aliyun.com (L. Fang).

https://doi.org/10.1016/j.matlet.2018.05.124
0167-577X/

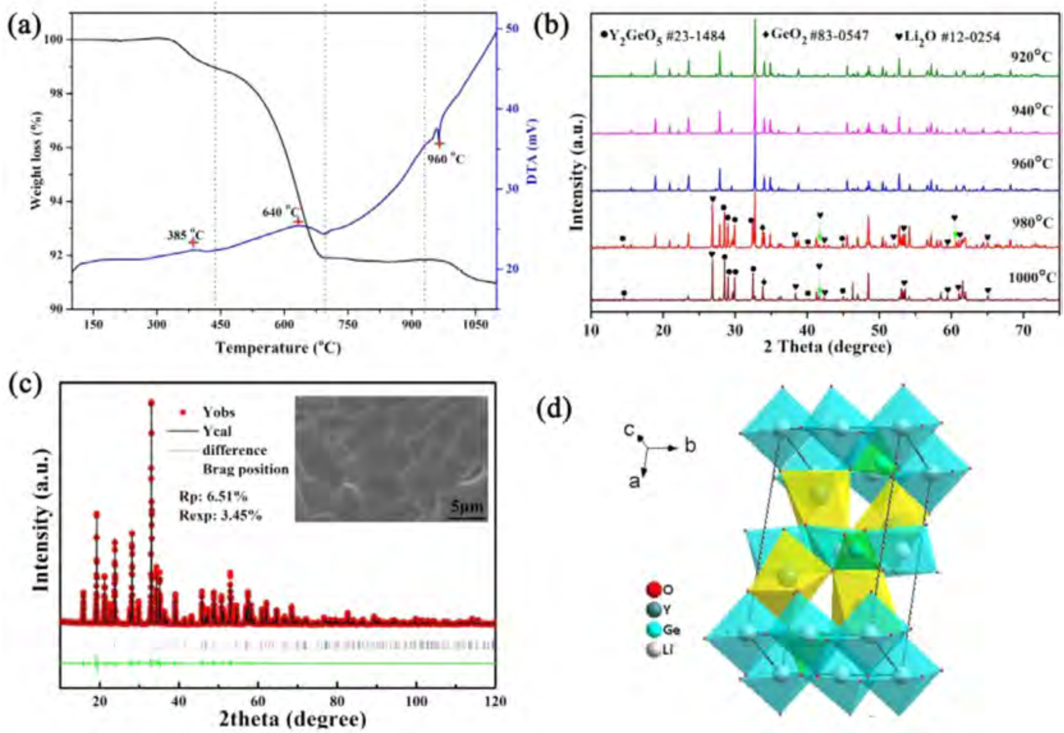

Fig. 1. (a) TGA/DSC curves of the mixture of raw powders; (b) XRD patterns of $LiYGeO_4$ ceramics; (c) Rietveld refinement and the SEM image on the sample sintered at 940 °C; (d) crystal structure of $LiYGeO_4$.

3. Results and discussion

Fig. 1a displays the TG and DTA curves on the as-milled raw powders. Three loss steps with a total weight loss of 9.3% are observed in the TG curves. An exothermic peak located at 385 °C with 1.3% weight loss was due to the decomposition of the organic species and volatilization of the adsorbed water introduced from the milling process. Similar phenomena were previously reported in the synthesis of $Mg_{0.95}Zn_{0.05}TiO_3$ and $Ba(Co_{0.7}Zn_{0.3})_{1/3}Nb_{2/3}O_3$ [13,14]. The second weight loss of 7.2% between 440 and 680 °C, accompanied by another exothermic peak at 640 °C, was ascribed to the chemical reaction of reactants. The third weight loss in the TG curve was just 0.8% but with a remarkable endothermic peak in the DTA curve at 960 °C, which probably corresponded to the thermal decomposition of $LiYGeO_4$.

XRD patterns of the as-sintered ceramics at different temperatures are shown in Fig. 1b. When sintered at 920–960 °C, $LiYGeO_4$ crystallized in a single orthorhombic phase with a space group *Pnma* (62) within the limitation of the XRD. However, additional peaks belonging to Y_2GeO_5, GeO_2, and Li_2O evidently appeared at 980 °C. These results indicate the structural instability of $LiYGeO_4$ that decomposes at the elevated temperature which is expressed as $2LiYGeO_4 \overset{Heat}{\rightarrow} Y_2GeO_5 + GeO_2 + Li_2O$. The analysis obtained from the XRD patterns coincides well with the thermal analysis.

Fig. 1c displays the Rietveld refinement (based on the CIF data No. SD031487) plots of the 940 °C-sintered sample. The low residual factors (R_{wp} = 9.03%, R_{exp} = 3.45%, and R_p = 6.51%) combined with the good match between the observed and calculated XRD patterns verified the phase purity. The refined lattice parameter and unit cell volume were refined as a = 11.3568(4) Å, b = 6.4024 (2), c = 5.1072(4), and V = 371.35(4) $Å^3$, respectively. A dense and homogeneous microstructure with clear grain boundary is observed (Fig. 1c) for the 940 °C-sintered samples, with average grain size about 7 μm. Fig. 1d shows the schematic framework of the crystal structures of $LiYGeO_4$, composed of $[GeO_4]$ tetrahedra, $[LiO_6]$ and $[YO_6]$ octahedra. The edge-sharing $[LiO_6]$ octahedra form a chain along b axis, one of which is alternating edge-linked by $[GeO_4]$ tetrahedra to another chain, resulting in layers parallel to (1 0 0) plane and $[YO_6]$ octahedra are the consecutive layers between two successive layers.

Fig. 2 illustrates the room-temperature Raman spectra of $LiYGeO_4$ ceramics, and factor group analysis indicated that the $LiYGeO_4$ crystal possessed 36 Raman-active vibrational modes as follows:

$$\Gamma_{Raman} = 11A_g + 7B_{1g} + 11B_{2g} + 7B_{3g} \quad (2)$$

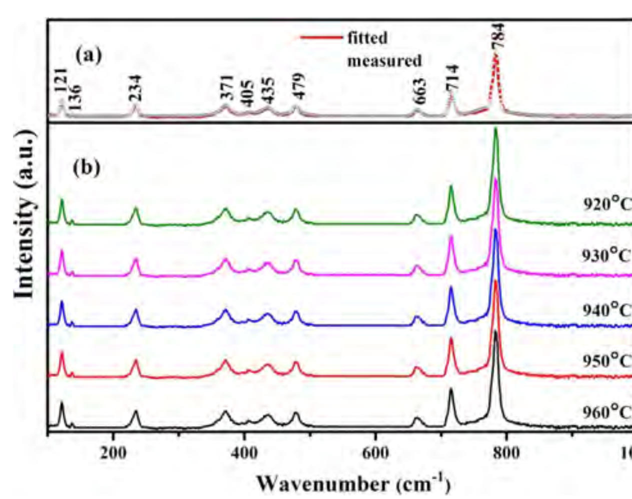

Fig. 2. Room-temperature Raman spectrum for the $LiYGeO_4$ samples in the range of 100–1000 cm^{-1} and fitting results on the sample sintered at 940 °C as a representative.

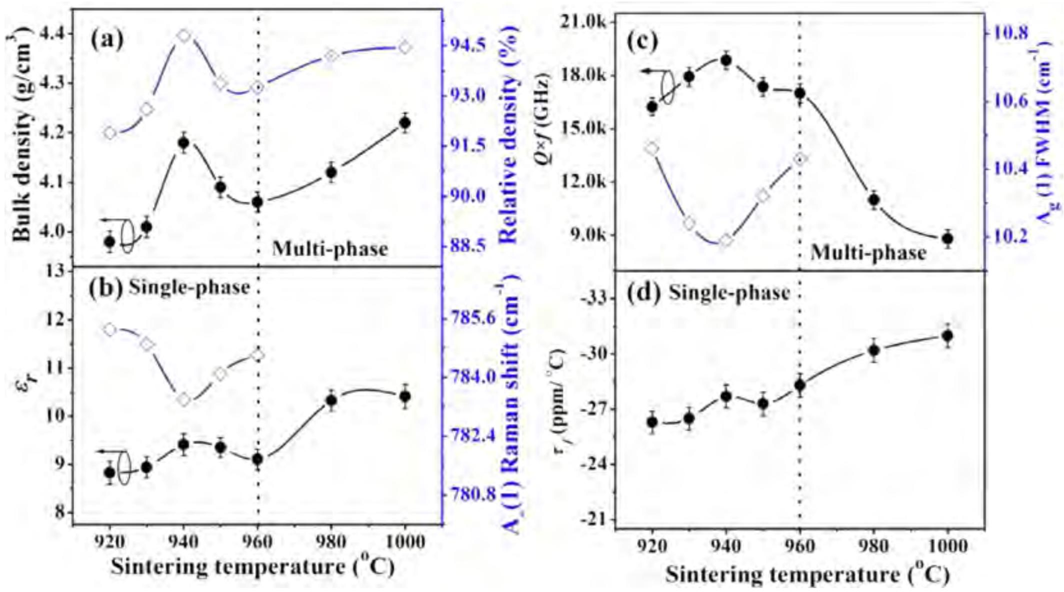

Fig. 3. Variations in the bulk density, relative density, and the relationship between $A_g(1)$ mode and microwave dielectric properties (ε_r, $Q \times f$, and τ_f values) of $LiYGeO_4$ ceramics as a function of sintering temperature.

However, only 22 Raman-active modes are distinguished based on the Lorentz fitting because of peak overlapping [6]. According to the previous study [15], the Raman modes lower than 300 cm^{-1} mainly originate from the translation vibration of cations. Among the modes between 350 and 600 cm^{-1}, four bands (371, 405, 435, 479 cm^{-1}) are assigned the asymmetric stretching vibrations of Y-O while the left modes are related to the bending and stretching vibrations of Ge-O bands [16]. The peaks observed at 714 and 784 cm^{-1} were assigned to the stretching vibration of $[GeO_4]$ and $[YO_6]$, respectively.

Fig. 3a shows the change of bulk density (ρ) and relative density of $LiYGeO_4$ ceramics versus sintering temperature (*Ts*). All the samples exhibit high relative density (>90% of the theoretical density (ρ_{th}), which ρ_{th} was 4.366 g/cm^3 for pure $LiYGeO_4$, 4.37 g/cm^3 for samples at 980 °C and 4.47 g/cm^3 for 1000 °C), showing "N" type curve with increasing temperature. The maximum values of the relative density 94.8% (~4.14 g/cm^3) was achieved at 940 °C. As *Ts* exceeded 960 °C, however, an exceptional increase in the density is observed, which is partly explained by the appearance of the second phase with higher density (e.g., 4.98 g/cm^3 for Y_2GeO_5 and 4.72 g/cm^3 for GeO_2) as a result of decomposition of $LiYGeO_4$. Besides, the low melting point of the second phases (e.g., GeO_2 ~1080 ± 45 °C) contributed to the densification of $LiYGeO_4$-based ceramics at elevated temperatures.

As shown in Fig. 3b and c, the variation trend in ε_r and $Q \times f$ value with increasing *Ts* to 960 °C is consistent to that of the relative density, and the optimum value with $\varepsilon_r = 9.41$ and $Q \times f =$ 18,860 GHz (at 12.8 GHz) was achieved at 940 °C, indicating the predominant role of density in microwave dielectric properties. However, the ε_r value increased to 10.45, and $Q \times f$ value decreased as *Ts* exceed 960 °C, which could be ascribed to the second phases. The inherent effects from the structural characteristics to the dielectric properties can be reflected with the help of Raman analysis using the high-energy stretch mode of the oxygen octahedrons $A_g(1)$ (with a wavenumber around 780 cm^{-1} at this work) [17,18]. As shown in Fig. 3b, the Raman shift of $A_g(1)$ mode presents an opposite variation tendency to the ε_r. Substantial Raman shift corresponds to high vibration energy of oxygen tetrahedron, which means rigid oxygen octahedron offering small space for cation vibration, resulting in lower ε_r. On the other hand, the variation in FWHM of $A_g(1)$ mode also displays an opposite trend to the $Q \times f$ value versus sintering temperature, as shown in Fig. 3c, verifying the fact that with increasing FWHM value the space for the lattice vibrations decreased and the inharmonic vibrations decrease, which in turn suppressed the intrinsic dielectric loss.

Table 1
Microwave dielectric properties of $(1-x)LiYGeO_4$-$xCaTiO_3$ $(0 \le x \le 0.045)$ ceramic.

x	S.T. (°C)	ε_r	$Q \times f$ (GHz)	τ_f (ppm/°C)
0	940	9.41 ± 0.03	17,600 ± 1600	−27.7 ± 1.80
0.015	940	9.73 ± 0.04	13,240 ± 1400	−18.9 ± 0.60
0.03	950	9.83 ± 0.03	12,940 ± 1600	−1.37 ± 0.70
0.045	950	9.88 ± 0.05	12,000 ± 1500	7.46 ± 1.20

As shown in Fig. 3d, the τ_f value remained relatively stable with a value of −27.7 ppm/°C below 960 °C, whereas it shifted to negative direction due to the unfavorable influence of the second phases. One of the effective method to tailor τ_f value is to add some materials with opposite-sign τ_f values. Owing to the structural stability of $CaTiO_3$, it not only could be used to design novel magnetic-dielectric composite [19] ceramic, but also used as a τ_f compensator in dielectric ceramics because of its large positive τ_f of +800 ppm/°C [20]. Thus, a series of $(1-x)LiYGeO_4$-$xCaTiO_3$ $(0 \le x \le 0.045)$ composite ceramics were fabricated. Table 1 summarizes the microwave dielectric properties. With $CaTiO_3$ addition the τ_f value increased from -27.7 to 7.46 ppm/°C accompanied by a slight increase in ε_r from 9.41 to 9.88, while the $Q \times f$ showed an obvious decrease. Specially, a composition with a near-zero τ_f value (~−1.37 ppm/°C) was achieved with 3 mol% $CaTiO_3$ addition.

4. Conclusions

A new microwave dielectric ceramic $LiYGeO_4$ with orthorhombic olivine structure was prepared. Thermal decomposition in $LiYGeO_4$ was verified and the effects of the second phase on microwave dielectric properties were observed. Dense ceramics and excellent microwave dielectric properties with $\varepsilon_r = 9.41$, $Q \times f =$ 18,860 GHz (at 12.8 GHz), and $\tau_f = -27.7$ ppm/°C were achieved.

A near-zero $\tau_f = -1.37$ ppm/°C with $\varepsilon_r = 9.83$ and $Q \times f = 12{,}940$ GHz (at 13.2 GHz) was obtained in the 0.97LiYGeO$_4$-0.03CaTiO$_3$ ceramic sintered at 950 °C for 6 h.

Acknowledgments

This work was financed by Natural Science Foundation of China (Nos. 51502047, 21561008, and 21761008). Author C.C. Li gratefully acknowledges the Guangxi Scholarship Fund of Guangxi Education Department.

Appendix A. Supplementary data

Supplementary data associated with this article can be found, in the online version, at https://doi.org/10.1016/j.matlet.2018.05.124.

References

[1] K.X. Song, S.Y. Wu, X.M. Chen, Mater. Lett. 61 (2007) 3357–3360.
[2] I.M. Reaney, D. Iddles, J. Am. Ceram. Soc. 89 (2010) 2063–2072.
[3] X.H. Zhou, M.J. Wang, Q.L. Zhang, H. Yang, L. Hu, D. Yu, Mater. Lett. 122 (2014) 9–12.
[4] W. Lei, W.Z. Lu, J.H. Zhu, X.H. Wang, Mater. Lett. 61 (2007) 4066–4069.
[5] M.T. Sebastian, H. Jantunen, Int. Mater. Rev. 53 (2008) 57–90.
[6] C.C. Li, H.C. Xiang, M.Y. Xu, Y. Tang, L. Fang, J. Eur. Ceram. Soc. 38 (2018) 1524–1528.
[7] S.P. Wu, Q. Ma, J. Alloys Compd. 567 (2013) 40–46.
[8] C.X. Chen, S.P. Wu, Y.X. Fan, J. Alloys Compd. 567 (2013) 40–46.
[9] N.H. Nguyen, J.B. Lim, S. Nahm, J.H. Paik, J.H. Kim, J. Am. Ceram. Soc. 90 (2010) 3127–3130.
[10] T. Tsunooka, M. Androu, Y. Higashida, H. Sugiura, H. Ohsato, J. Eur. Ceram. Soc. 23 (2003) 2573–2578.
[11] J. Li, L. Fang, H. Luo, J. Khaliq, Y. Tang, C.C. Li, J. Eur. Ceram. Soc. 36 (2016) 243–246.
[12] J.X. Bi, Y.J. Niu, H.T. Wu, Ceram. Int. 43 (2017) 7522–7530.
[13] A. Ullaha, Y. Iqbal, T. Mahmood, A. Mahmood, A. Naeem, M. Hamayun, Ceram. Int. 41 (2015) 15089–15096.
[14] B. Itaalit, M. Mouyane, J. Bernard, J. Reboul, D. Houivet, Ceram. Int. 41 (2015) 1937–1942.
[15] H.C. Xiang, L. Fang, W.S. Fang, Y. Tang, C.C. Li, J. Eur. Ceram. Soc. 37 (2017) 625–629.
[16] V.B.R. Boppana, N.D. Hould, R.F. Lobo, J. Solid State Chem. 184 (2011) 1054–1062.
[17] S.K. Singh, V.R.K. Murthy, Ceram. Int. 42 (2016) 7284–7289.
[18] Y. Wu, D. Zhou, J. Guo, L.X. Pang, H. Wang, X. Yao, Mater. Lett. 65 (2011) 2680–2682.
[19] D.V.M. Paiva, M.A.S. Silva, T.S. Ribeiro, I.F. Vasconcelos, A.S.B. Sombra, J.C. Góes, P.B.A. Fechine, J. Alloys Compd. 644 (2015) 763–769.
[20] M.A. Sanoj, M.R. Varma, J. Alloys Compd. 477 (2009) 565–569.